

# On Redundant Flagged Manipulators

Maria Alberich-Carramiñana, Federico Thomas, and Carme Torras  
*Institut de Robòtica i Informàtica Industrial (IRI) CSIC-UPC*  
*Llorens i Artigues 4-6, 08028-Barcelona, Spain*

**Abstract**—Flagged in-parallel manipulators are attractive because their singularity loci admit a well-behaved decomposition, with a unique topology irrespective of the metrics of each particular design. In this paper, this topology is formally derived and all the cells, in the configuration space of the platform, of dimension 6 (non-singular) and dimension 5 (singular), together with their adjacencies, are worked out in detail. This characterization of the singularity loci is useful to come up with designs which admit control strategies free of singularities. In particular, it is shown that by adding an extra leg to any flagged manipulator, the resulting 7-leg structure admits a control strategy (by appropriately choosing which leg remains passive) that completely avoids singularities.

**Index Terms**—Parallel manipulators, kinematics singularities, manipulator design, stratification, flag manifold.

## I. INTRODUCTION

An important shortcoming of current parallel manipulators is that, in general, they are forced to operate in reduced workspaces so as to avoid singular configurations. Thus, research on parallel manipulators has led to eliminating singularities by adding actuators either in an existing or an added leg, that is, by introducing redundancy. Merlet has already outlined the key concepts to be considered in designing and using a redundant parallel manipulator [10].

Adding legs, instead of adding more actuators to existing legs, can cause more leg interference, which is already an important limitation for the use of parallel manipulators. Nevertheless, a benefit is obtained: enhanced robustness to actuator failure. In other words, if one actuator fails, the mechanism could still function in a reduced workspace by leaving the failing leg passive.

Since adding a redundant leg decreases the dimension of the singularity space [4], some research has been carried out to determine where to locate this leg to effectively decrease or even to eliminate the singularity surface [13]. The result has been several successful implementations of redundant parallel manipulators with extra legs [9], [18]. It is worth noting here that the idea of using redundant actuators is closely related to that of adding extra sensors to obtain unique closed-form solutions for the forward kinematics of parallel manipulators (see, for example [2], and the references therein). Thus, the literature on the location of extra sensors in parallel manipulators is also an important source of inspiration to decide where to locate extra actuators.

In a 7-leg in-parallel manipulator, by switching which leg remains passive, the distribution of singularities across

the configuration space of the platform with respect to the base (C-space, for short) changes, and we can exploit this change for singularity avoidance. To this aim, it is necessary to obtain a complete and precise characterization of the singularity loci of the involved manipulators which, in general, is not an easy task. Fortunately, for the class of Stewart-Gough platforms known as *flagged* parallel manipulators, their singularity loci has been shown to have a well-behaved structure inherited from the stratification of the flag manifold [17]. Following this result, in this paper we characterize in detail the C-space of flagged manipulators in terms of cells of dimension 6 (non-singular) and dimension 5 (singular), together with their adjacencies. Then, adding an extra leg and switching actuation implies converting a flagged manipulator instance into another, and, consequently, changing the location of the 5D cells. The placement of the extra leg can be designed so that 5D cells (singularity loci) of the two manipulator instances have at most a 4D intersection. This means that the C-space of the resulting manipulator with switched control has singularity loci of at most dimension 4, which can easily be avoided in practice.

This paper is structured as follows. The next section gives an introductory overview to flagged manipulators. Section III deals with the stratification of the flag manifold. Then, Section IV discusses how this stratification induces a stratification of the singularity loci of flagged manipulators. The topology of the cells of dimension 6 (non-singular) and dimension 5 (singular) is worked out in detail in Section V. Section VI discusses the problem of adding an extra leg to a flagged manipulator which, using a switching strategy, would permit minimizing the effect of singularities. Finally, Section VII provides some conclusions and points that deserve further attention.

## II. FLAGGED MANIPULATORS

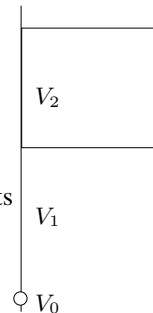


Fig. 1. A flag consists of a point,  $V_0$ , a line,  $V_1$ , and a plane,  $V_2$ , such that  $V_0 \subset V_1 \subset V_2$ .

This research has been partially supported by the Spanish Committee for Science and Technology (CICYT), project DPI2004-07358, and the Catalan Research Commission, through the Robotics and Control group.

Let us consider a plane, a line and a point so that the point is contained in the line, and the line in the plane. This geometric entity is called a flag (Fig. 1). A parallel manipulator whose singularities can be described in terms of incidences between two flags is called a flagged manipulator. The relevance of these manipulators derives from the fact that their singularity analysis is quite simple because:

- 1) the topology of their singularity spaces is the same for all members of the family irrespective of changes in their kinematic parameters.
- 2) their singularity spaces can be easily decomposed into manifolds, or cells, forming what in algebraic geometry is called a “stratification,” derived from that of the flag manifold.
- 3) each cell can be characterized using a single local chart whose coordinates directly correspond to uncoupled translations and/or rotations in the workspace of the manipulator.
- 4) any path connecting two assembly modes passes through a singularity (note that this assertion is not true in general [8]).

Next, let us elaborate on how the whole family of flagged manipulators is obtained in a rather intuitive way.

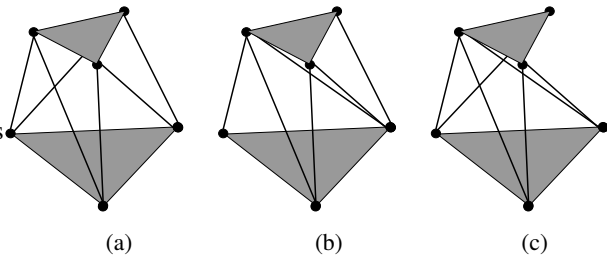


Fig. 2. The three possible architectures for the 3-3 parallel manipulators.

Let us consider the set of in-parallel manipulators whose leg end-points merge into three multiple spherical joints both in the base and the platform. There are only three possible architectures for this kind of manipulators, also known as 3-3 manipulators (Fig. 2). One of them corresponds to the well-known octahedral manipulator [Fig. 2(a)] whose forward kinematics is not solvable in closed-form [5]. On the contrary, the forward kinematics of the other two can be solved by a sequence of three consecutive trilaterations [7], [3], [15] leading to 8 solutions, or assembly modes.

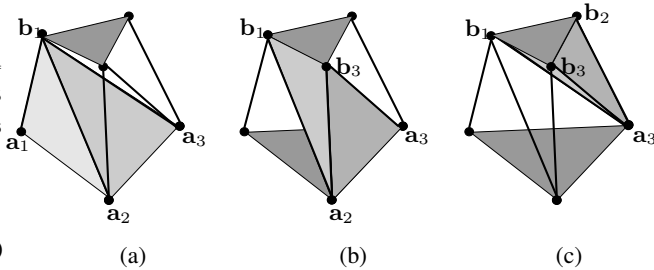


Fig. 3. The tetrahedra involved in the computation of the forward kinematics of the parallel manipulator in Fig. 2(b).

Now, let us concentrate our attention on the forward kinematics of the parallel manipulator in Fig. 2(b). Given the lengths of the segments  $a_1b_1$ ,  $a_2b_1$ , and  $a_3b_1$ , there are two possible mirror locations for  $b_1$  with respect to the plane defined by  $a_1$ ,  $a_2$ , and  $a_3$  [Fig. 3(a)]. Once one of these two solutions for  $b_1$  is chosen,  $a_2$ ,  $a_3$ ,  $b_1$  and  $b_3$  define another tetrahedron with known edge lengths [Fig. 3(b)]. Again, there are two possible mirror locations for  $b_3$ , in this case with respect to the plane defined by  $a_2$ ,  $a_3$ , and  $b_1$ . Finally, after choosing one of the two solutions,  $a_3$ ,  $b_1$ ,  $b_2$ , and  $b_3$  define another tetrahedron with known edge lengths [Fig. 3(c)]. In this case there are two mirror locations for  $b_2$  with respect to the plane defined by  $b_1$ ,  $b_3$  and  $a_3$ . We conclude that if, and only if, the points in the sets  $\{a_1, a_2, a_3, b_1\}$ ,  $\{a_2, a_3, b_1, b_3\}$ , and  $\{a_3, b_1, b_2, b_3\}$  form non-degenerate tetrahedra, there are eight possible configurations for the moving platform compatible with a given set of leg lengths. Otherwise, the parallel manipulator is in a singularity [16]. Alternatively, we can say that the manipulator is in a singularity if  $b_1$  is on the base plane, the lines defined by  $a_2a_3$  and  $b_1b_3$  intersect, or  $a_3$  is on the platform plane. This reinterpretation is important because it is not expressed in terms of leg locations but directly in terms of points and edges attached to either the base or the platform. Therefore, if two flags are placed on the manipulator base and platform as shown in Fig. 4, then the manipulator singularities coincide with flag configurations in which either the vertex of one flag lies on the plane of the other flag or the two flag lines intersect.

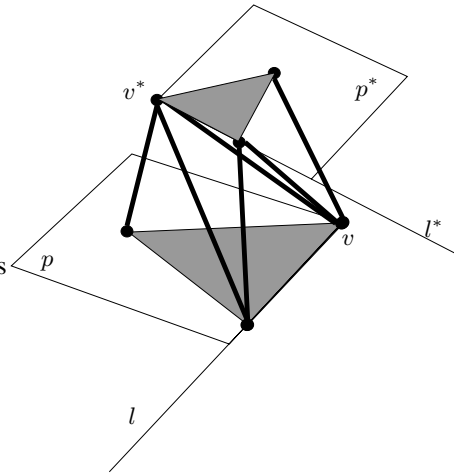


Fig. 4. The basic flagged manipulator and its attached flags.

In what follows, the parallel manipulator in Fig. 4 is called the *basic flagged manipulator*. Moreover,  $v$ ,  $l$  and  $p$  will denote the point, line and plane of the flag attached to the base, while the same letters with an asterisk will stand for the same flag features of the flag attached to the platform.

It is possible to apply the local transformation shown in Fig. 5a on the location of the leg endpoints of an in-parallel manipulator with multiple spherical joints so that its sin-

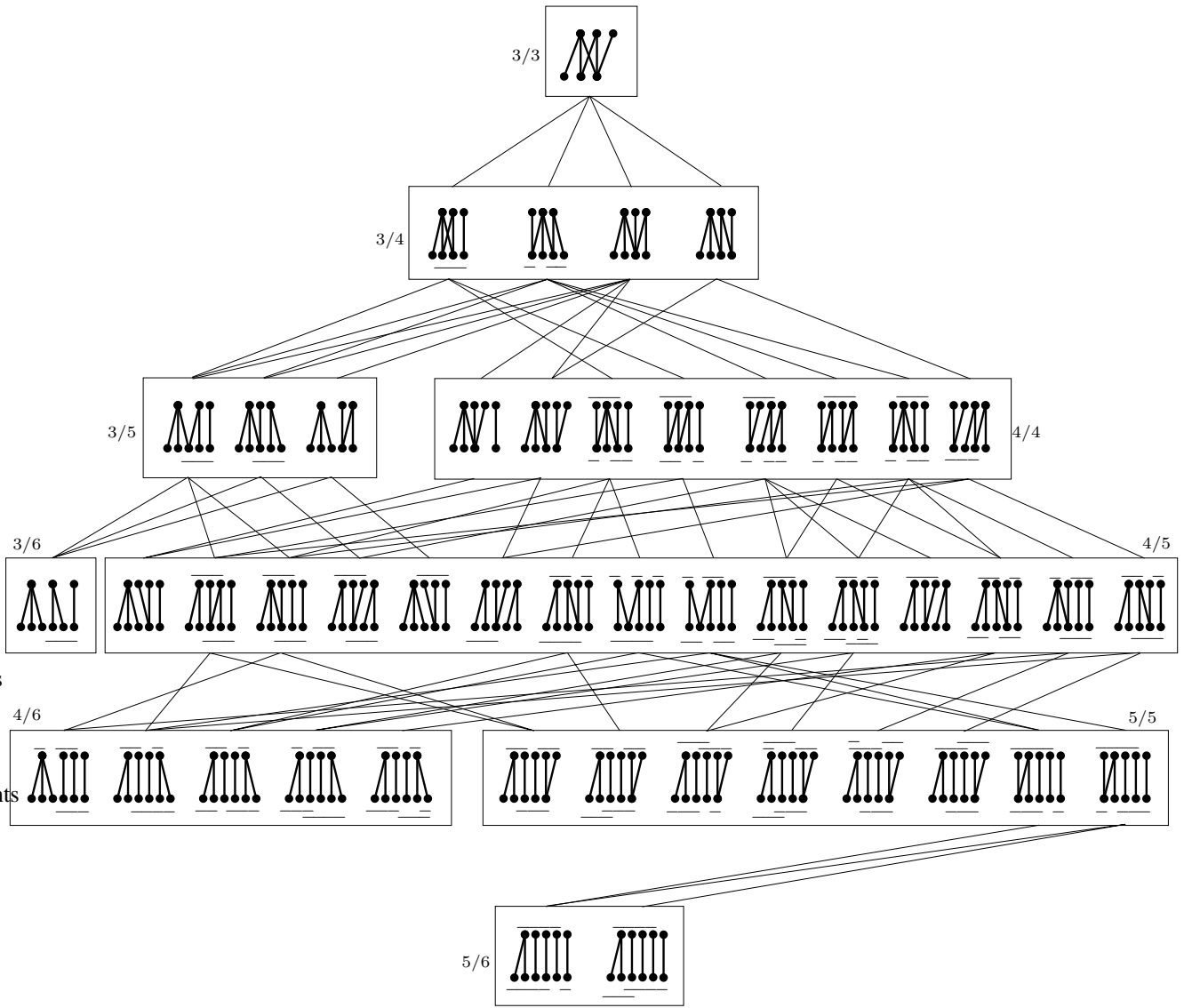


Fig. 6. The whole family of flagged manipulators expanded from the basic one by applying the transformation in Fig. 5a. Segments, next to either the base or the platform, indicate the endpoints that should be kept aligned.

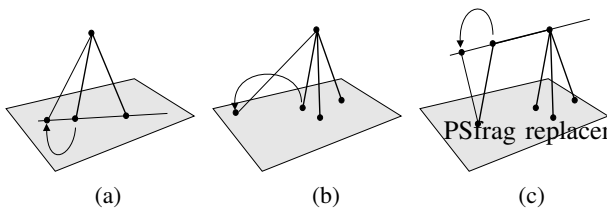


Fig. 5. Local transformation on the location of a leg endpoint that leave singularities invariant (a), and other local transformations that can be obtained by applying twice (b) and five times (c) the transformation in (a).

gularities remain invariant. Other local transformations can be derived from it (Fig. 5b and 5c). These transformations permit expanding the whole family of flagged manipulators shown in Fig. 6.

As an example, Fig. 7 shows how the 3/2 Hunt-Primrose manipulator [7] can be derived from the basic flagged

manipulator by applying a sequence of four of these transformations.

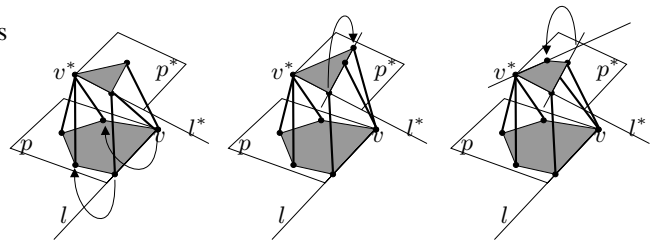


Fig. 7. The 3/2 Hunt-Primrose manipulator is a flagged manipulator because it can be obtained by applying a sequence of four local transformations to the basic flagged manipulator. Notice how the attached flags remain invariant under these transformations.

The combinatorics of the singularities of flagged manipulators was exploited in [17], while here we go on to derive the topology of the singularity locus in terms of the 6D and

5D cells together with their adjacencies. To this end, we should now proceed more formally.

### III. FROM PROJECTIVE FLAGS TO AFFINE FLAGS

*Definition 1 (Flag):* A flag in projective space  $\mathbb{P}^3$  is a sequence  $V_0 \subset V_1 \subset V_2 \subset \mathbb{P}^3$  of projective subspaces such that  $\dim(V_i) = i$ .  $V_0, V_1$  and  $V_2$  are called the *flag features*.

The Euclidean space  $\mathbb{R}^3$  can be viewed as a subspace of  $\mathbb{P}^3$  via  $\mathbb{R}^3 \cong \mathbb{P}^3 \setminus \Pi_\infty$ , where  $\Pi_\infty$  stands for the plane at infinity. The flags we will be concerned with are the *affine flags*, that is, flags  $V_0 \subset V_1 \subset V_2 \subset \mathbb{P}^3$  satisfying  $V_0 \not\subset \Pi_\infty$ .

In what follows, we make a slight abuse of language by identifying affine subspaces of dimensions 0, 1, and 2, in projective space  $\mathbb{P}^3$  not contained in  $\Pi_\infty$  with points, lines, and planes, in Euclidean space  $\mathbb{R}^3$ .

*Definition 2 (Flag manifold):* The flag manifold  $\mathcal{Flag}(4)$  is the set of all flags in  $\mathbb{P}^3$ . Let  $\mathcal{F}_A(\mathbb{P}^3)$  denote the subset of the affine flags in  $\mathcal{Flag}(4)$ .

Let  $v \subset l \subset p$  be a fixed *reference flag*. The flag manifold  $\mathcal{Flag}(4)$  admits the following cell decomposition or stratification:

$$\mathcal{Flag}(4) = \cup_{w \in \sum_4} B^w, \quad (1)$$

where  $B^w$  is the set of all the flags whose flag features have incidence relations with the reference flag determined by the permutation  $w \in \sum_4$ , with  $\sum_4$  standing for the set of permutations of 4 elements [6].

Each cell  $B^w$  is isomorphic to  $\mathbb{R}^{\text{length}(w)}$  and hence it is connected. Furthermore in the stratification (1), two cells of consecutive dimensions are adjacent if and only if there is a single transposition between their associated permutations. This leads to an algorithmic procedure to derive the graph of cells for the flag manifold, as was displayed in [17]. Fig. 8 shows the cells of dimensions 6 and 5 and their adjacencies. The rectangle represents the 6D cell  $B^{(4,3,2,1)}$ , while the ellipses are the 5D cells:  $B^{(4,3,1,2)}$ ,  $B^{(3,4,2,1)}$  and  $B^{(4,2,3,1)}$ . Each 5D cell is labelled also with  $v - p^*$ ,  $p - v^*$  and  $l \cdot l^*$ , respectively, which characterize the incidence relations between the flag features of the flags  $v^* \subset l^* \subset p^*$  in each cell and the reference flag. A hyphen between two elements denotes that one is included in the other, and a dot means that they meet at a single point.

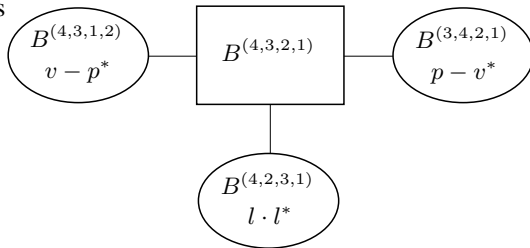


Fig. 8. Stratification of the flag manifold: the rectangle represents the 6D cell, and the ellipses are the 5D cells.

The stratification of the flag manifold  $\mathcal{Flag}(4)$  induces a stratification of the subset of affine flags  $\mathcal{F}_A(\mathbb{P}^3)$ . Indeed,

after removing the plane at infinity  $\Pi_\infty$ , the resulting decomposition is still a stratification, and some cells (those whose associated permutations don't start with a 1) are split into two connected components [1]. Fig. 9 shows the cells of dimensions 6 and 5 of  $\mathcal{F}_A(\mathbb{P}^3)$  and their adjacencies. The rectangles represent the two 6D cells  $B_+^{(4,3,2,1)}$  and  $B_-^{(4,3,2,1)}$ , while the ellipses are the six 5D cells:  $B_\varepsilon^{(4,3,1,2)}$ ,  $B_\varepsilon^{(3,4,2,1)}$  and  $B_\varepsilon^{(4,2,3,1)}$ , with  $\varepsilon \in \{+, -\}$ . For the sake of clarity, each 5D cell is labelled with  $(v - p^*)^\varepsilon$ ,  $(p - v^*)^\varepsilon$  and  $(l \cdot l^*)^\varepsilon$ , respectively, to make explicit the incidence relations between the flag features of the flags in each cell and those of the reference flag.

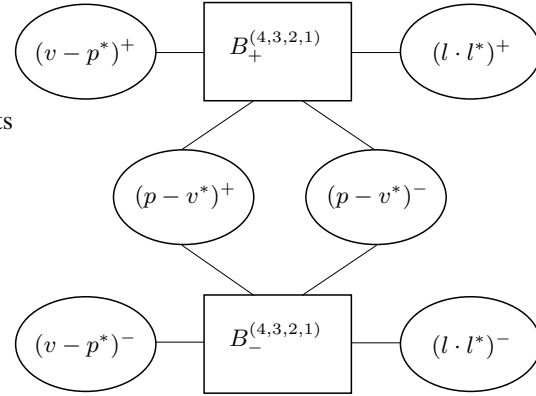


Fig. 9. Stratification of the set of affine flags: the rectangles represent the 6D cells, and the ellipses are the 5D cells.

The stratification of the set of affine flags induces a decomposition of the C-space of flagged manipulators, which we work out in detail in the next section.

### IV. FROM THE FLAG MANIFOLD STRATIFICATION TO PARALLEL MANIPULATOR SINGULARITIES

Given a flag  $\mathcal{V}^* = (v^*, l^*, p^*)$  attached to the basic flag manipulator as in Fig. 4 (and, in general, to any other member of the family of flagged manipulators), we consider a reference frame having  $v^*$  as origin,  $l^*$  as the  $x$  axis, and  $p^*$  as the  $xy$  plane. This flag remains invariant when a rotation of  $\pi$  radians about any of the three coordinate axes is applied. Formally, the group of Euclidean transformations leaving the flag invariant is  $\mathcal{H}_{\mathcal{V}^*} = \{\mathbf{I}, \mathbf{R}_x, \mathbf{R}_y, \mathbf{R}_z\}$ , where  $\mathbf{I}$  is the identity transformation, and  $\mathbf{R}_k$  stands for a rotation of  $\pi$  radians about the  $k$ -axis. Let us mention that  $\mathcal{H}_{\mathcal{V}^*}$  is one of the representations of the well-known Klein four-group, since  $\mathbf{R}_x \mathbf{R}_y = \mathbf{R}_y \mathbf{R}_x = \mathbf{R}_z$ ,  $\mathbf{R}_x \mathbf{R}_z = \mathbf{R}_z \mathbf{R}_x = \mathbf{R}_y$ , and  $\mathbf{R}_y \mathbf{R}_z = \mathbf{R}_z \mathbf{R}_y = \mathbf{R}_x$ .

Now, let us fix a reference frame at the base of the flagged manipulator attached to the reference flag  $\mathcal{V} = (v, l, p)$  (and oriented in the same way as the frame previously fixed at the platform). Then, a manipulator configuration is described as  $\mathbf{q} \in \mathbb{R}^3 \times \text{SO}(3)$ , relating the platform frame to the base frame. Given one such manipulator configuration  $\mathbf{q}$ , we can characterize the set of 4 manipulator configurations yielding this same flag

configuration as follows:

$$\left\{ \mathbf{T}\mathbf{q} \mid \mathbf{T} \in \mathcal{H}\mathcal{V}_{\mathbf{q}}^* \right\}, \quad (2)$$

where  $\mathcal{V}_{\mathbf{q}}^*$  is the flag associated with the platform in configuration  $\mathbf{q}$ . This gives a four-fold covering morphism  $\pi : \mathbb{R}^3 \times \text{SO}(3) \rightarrow \mathcal{F}_{\mathcal{A}}(\mathbb{P}^3)$  sending  $\mathbf{q}$  to  $\mathcal{V}_{\mathbf{q}}^*$  [14]. Therefore, with each relative configuration of *two flags*, we can associate 4 relative configurations of the platform and base.

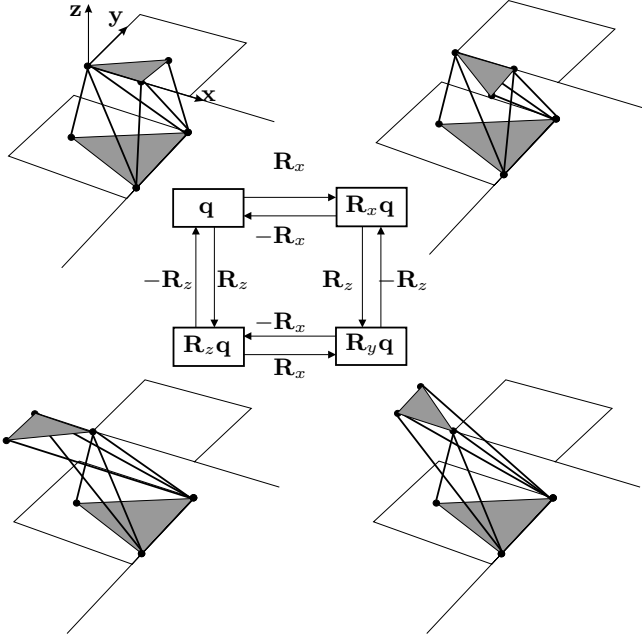


Fig. 10. The four platform configurations sharing the same flag, obtained by rotating  $\pi$  radians about its reference axes.

Figure 10 shows the four platform configurations sharing the same flag  $\mathcal{V}_{\mathbf{q}}^*$ , namely  $\mathbf{q}$ ,  $\mathbf{R}_x \mathbf{q}$ ,  $\mathbf{R}_y \mathbf{q}$ , and  $\mathbf{R}_z \mathbf{q}$ .

Summarizing, the configuration space of the manipulator can be seen as a 4-fold covering of the set of affine flags. The interesting property is that it thus inherits the nice structure of the latter, as detailed in the next section.

## V. THE TOPOLOGY OF SINGULARITIES

The covering morphism  $\pi$  induces a stratification of  $\mathbb{R}^3 \times \text{SO}(3)$ , and hence of the singularity locus of the flagged manipulator, from the stratification of  $\mathcal{F}_{\mathcal{A}}(\mathbb{P}^3)$  obtained in the preceding section. In particular, Equation (2) provides a procedure to unfold the stratification of the affine flags so as to obtain a useful decomposition of the C-space of the manipulator.

Due to the 4 degree of  $\pi$ , the two 6-dimensional disjoint cells in  $\mathcal{F}_{\mathcal{A}}(\mathbb{P}^3)$  correspond in  $\mathbb{R}^3 \times \text{SO}(3)$  to 8 6D cells, that is, 8 connected components of the non-singular manipulator configurations, which (by connectness arguments) must correspond to the 8 assembly modes of the flagged manipulators. Hence there are 8 connected components of non-singular configurations in C-space. To visualize these 8 cells see Fig. 10: besides the four platform configurations sharing the same flag  $\mathcal{V}_{\mathbf{q}}^*$ , we could draw the

other four configurations corresponding to their images by the specular reflection through the plane of the base.

Now, how are these 8 cells packed together in C-space? Owing to the placement chosen for the two flags in the manipulator, the 5D cells provide a decomposition of the singularity locus.

Recall that there are 3 5-dimensional cells in  $\mathcal{F}lag(4)$ , which correspond to the cases in which point  $v^*$  of the platform lies on the base plane, point  $v$  of the base lies on the platform plane, and lines  $l$  and  $l^*$  intersect. Restricted to  $\mathcal{F}_{\mathcal{A}}(\mathbb{P}^3)$  they split off into 6 5-D cells. Due to the 4 degree of  $\pi$ , this leads in  $\mathbb{R}^3 \times \text{SO}(3)$  to 24 5D cells. We say that a 5D cell is of type  $v^* - p$ ,  $v - p^*$  or  $l \cdot l^*$  if it is one of the connected components of the inverse image of a cell  $(v^* - p)^\varepsilon$ ,  $(v - p^*)^\varepsilon$  or  $(l \cdot l^*)^\varepsilon$ , respectively, for some  $\varepsilon \in \{+, -\}$ .

By resorting to the theory of path lifting [1], the adjacencies between these 8 6D cells and 24 5D cells can be derived, resulting in the graph shown in Fig. 11. The rectangles represent the 8 6D connected components of C-space of non-singular configurations, while the ellipses are the 5D manifold patches of singular configurations separating these components. The 4 multiplicity appears clearly at this level as well. Note that each non-singular region has the same structure, being bounded by 6 singular regions, two of type  $l \cdot l^*$ , two of type  $v - p^*$ , and two more of type  $p - v^*$ . To characterize each 6D cell we can use a triple of signs corresponding to the orientation of the three tetrahedra appearing in Fig. 3.

## VI. ADDING AN EXTRA LEG TO REMOVE SINGULARITIES

Assuming that the platform of a flagged manipulator doesn't cross the plane of its base, its C-space consists of four 6D cells (corresponding to the four forward kinematic solutions for a given set of leg lengths), separated by eight 5D (singular) cells. Thus, only the cells appearing in the top half of Fig. 11 need to be considered.

To avoid singularities, manipulators are often made to operate within just one 6D cell. In this section we show that, by adding an extra leg and using switched control, the 5D singularity cells can be removed and, consequently, the operation workspace of the resulting redundant flagged manipulator becomes enlarged by a factor of four.

Given the basic flagged manipulator shown in Fig. 4, there are two ways of placing an extra leg, namely .

To the former of these 7-leg designs, we can attach a first pair of flags  $(v_1, l, p)$  and  $(v^*, l_1^*, p^*)$  in the same way as in Fig. 4, and then a second pair of flags  $(v_2, l, p)$  and  $(v^*, l_2^*, p^*)$ , yielding the flag arrangement displayed in Fig. 12. Now, if the extra leg remains passive, we have just a basic flagged manipulator, with the former pair of attached flags. Contrarily, if the leg symmetric to the extra leg (involving the other endpoints of arity 3 in the base and 2 in the platform) remains passive, then we have another basic flagged manipulator, whose singularity locus

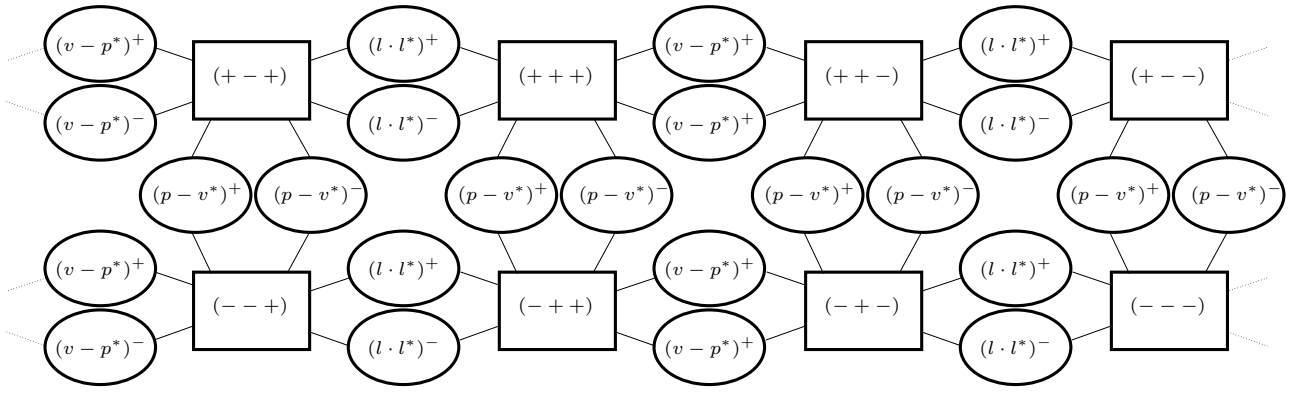


Fig. 11. The graph shows the topology of C-space for flagged manipulators. The rectangles represent the 6D cells of C-space non-singular configurations which correspond to the eight different assembly modes, while the ellipses are the 5D cells of singular configurations.

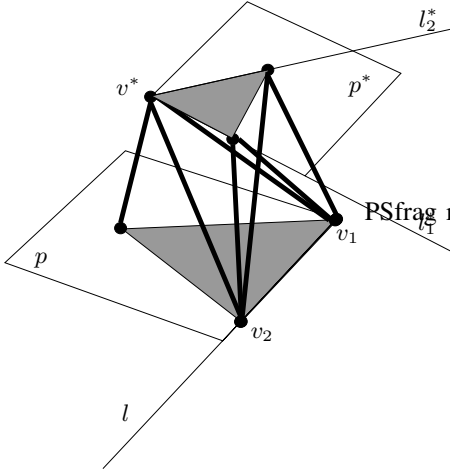


Fig. 12. The basic redundant flagged manipulator and the two pairs of attached flags:  $(v_1, l, p)$  and  $(v_2, l, p)$  attached to the base, and  $(v^*, l_1^*, p^*)$  and  $(v^*, l_2^*, p^*)$  attached to the platform.

is characterized by the second pair of flags  $(v_2, l, p)$  and  $(v^*, l_2^*, p^*)$ .

The interesting point is that the singularity loci of these two component basic manipulators intersect only on 4D sets. To see this, have a look at Table I, where the intersections of the 5D singularity manifolds arising from the two pairs of flags are recorded. Note that the only 5D intersection is  $p - v^*$ , and this is removed by the assumption that the platform cannot cross the plane of the base. Therefore, we have only to consider the first two rows and columns in the table, which show that only two types of 4D intersections appear: when the platform plane contains the base line, or when the platform line contains the base vertex. Since these 4D singularities are well characterized, they can be easily circumvented using an adequate control strategy.

Note that the 7-leg manipulator obtained by interchanging the roles of platform and base doesn't have this interesting property, since in this case the last two rows and columns in the table must be considered instead, and the  $p - v^*$  5D singularity remains.

Concerning the alternative design ~~3-2-1~~, there is no possibility to move the vertex of neither the platform flag nor the base flag, and therefore one of the 5D singularities  $v - p^*$  or  $p - v^*$  necessarily remain.

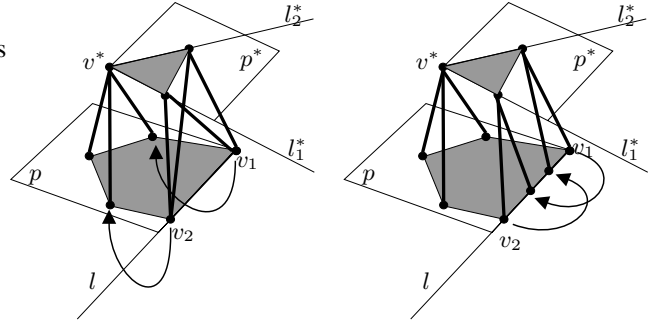


Fig. 13. A 3-2-2 manipulator is obtained by applying local transformations to the basic redundant flagged manipulator in Fig. 12.

In sum, there is only one 7-leg basic flagged configuration of interest, namely that shown in Fig. 12. From this, and using the transformations in Fig. 5, all redundant flagged parallel manipulators can be derived, as was done for non-redundant flagged manipulators in Fig. 6. An example is shown in Fig. 13, where a 3-2-2 manipulator is obtained by using four transformations.

## VII. CONCLUSION

We have proved that the configuration space of flagged manipulators can be decomposed into eight connected components (cells of dimension 6), corresponding to the eight possible assembly modes, separated by singularities (cells of dimension 5 and lower). The topology of all cells of dimension 6 and 5 has been formally derived in detail.

Adding an extra leg to a flagged manipulator and switching actuation implies converting a flagged manipulator instance into another, and, consequently, changing the location of the 5D cells. Then, the placement of the extra leg can be designed so that 5D cells of the two manipulator instances have at most a 4D intersection. This means that the resulting manipulator with switched control has a singularity locus of at most dimension 4. In order to

TABLE I  
INTERSECTIONS OF THE SINGULARITY 5D MANIFOLDS FOR TWO PAIRS OF FLAGS.

	$v_2 - p^*$	$l \cdot l_2^*$	$p - v^*$
$v_1 - p^*$	$l - p^*$	$(v_1 - l_2^*) \cup (l - p^*)$	$\overline{v_1} - p^*$
$l \cdot l_1^*$	$(v_2 - l_1^*) \cup (l - p^*)$	$l - p^*$	$(l - v^*) \cup (p - l_1^*)$
$p - v^*$	$\overline{v_2} - p^*$	$(l - v^*) \cup (p - l_2^*)$	$p - v^*$

characterize all possible redundant flagged manipulators, we have applied the same strategy used for the non-redundant case. First, all redundant 3-3 architectures have been explored to conclude that only one of them has interest from the perspective of flagged manipulators. Then, it has been shown how all possible redundant flagged manipulators could be derived from it using one simple local transformations on the leg endpoint locations.

The results presented herein have direct application to wire-base tracking devices. Indeed, this kind of devices are forced to operate in reduced workspaces so as to avoid singular configurations and wire wrapping problems [16]. The effect of singularities can be minimized by introducing redundant wires, and wire wrapping problems by rearranging wire ends –to adapt the device to a particular application or experiment– without modifying the singularity landscape. We have presented effective techniques to solve both problems.

#### REFERENCES

- [1] M. Alberich-Carramiñana, V. González, and C. Torras, “The topology of singularities of flagged parallel manipulators,” *IRI Technical Report*, 2005 (available at <http://www-iri.upc.es/people/torras>).
- [2] I. Bonev, J. Ryu, S.-G. Kim, and S.-K. Lee, “A closed-form solution to the direct kinematics of nearly general parallel manipulators with optimally located three linear extra sensors,” *IEEE Trans. on Robotics*, Vol. 17, No. 2, pp. 148-156, 2001.
- [3] H. Bruyninckx, “Forward kinematics for Hunt-Primrose parallel manipulators,” *Mechanism and Machine Theory*, Vol. 34, pp. 657-664, 1999.
- [4] Dasgupta and T. Mruthyunjaya, “Force redundancy in parallel manipulators: Theory and practical issues,” *Mechanism and Machine Theory*, Vol. 33, No. 6, pp. 727-742, 1998.
- [5] D.M. Downing, A.E. Samuel, and K.H. Hunt, “Identification of the special configurations of the octahedral manipulator using the pure condition,” *The International Journal of Robotics Research*, Vol. 21, No. 2, pp. 147-160, 2002.
- [6] H. Hiller, *Geometry of Coxeter Groups*, Research Notes in Mathematics, Pitman Books, London, 1982.
- [7] K.H. Hunt and E.J.F. Primrose, “Assembly configurations of some in-parallel-actuated manipulators,” *Mechanism and Machine Theory*, Vol. 28, No. 1, pp. 31-42, 1993.
- [8] C. Innocenti and V. Parenti-Castelli, “Singularity-free evolution from one configuration to another in serial and fully-parallel manipulators,” *ASME 22<sup>nd</sup> Biennial Mechanisms Conference: Robotics, Spatial Mechanisms, and Mechanical Systems*, Vol. 45, pp. 553-560, 1992.
- [9] S. Kock and W. Schumacher, “A parallel x-y manipulator with actuation redundancy for high-speed and active-stiffness applications,” *Proc. of the Int. Conf. on Robotics and Automation*, pp. 2295-2300, 1998.
- [10] J.-P. Merlet, “Redundant parallel manipulators,” *Laboratory Robotics and Automation*, Vol. 8, No. 1, pp. 17-24, 1996.
- [11] J.-P. Merlet, *Parallel Robots*, Springer, 2000.
- [12] D. Monk, “The Geometry of Flag Manifolds,” *Proc. of the London Mathematical Society*, Vol. 9, No. 9, 1959.
- [13] L. Notash and R. Podhorodeski, “Forward displacements analysis and uncertainty configurations of parallel manipulators with a redundant branch,” *Journal of Robotic Systems*, Vol. 13, No. 9, pp. 587-601, 1996.
- [14] P. Sankaran and P. Zvengrowski, “Stable parallelizability of partially oriented flag manifolds II,” *Can. J. Math*, Vol. 49, No. 6, pp. 1323-1339, 1997.
- [15] S.-K. Song and D.-S. Kwon, “A tetrahedron approach for a unique closed-form solution of the forward kinematics of six-dof parallel mechanisms with multiconnected joints,” *Journal of Robotic Systems*, Vol. 19, No. 6, pp. 269-281, 2002.
- [16] F. Thomas, E. Ottaviano, L. Ros, and M. Ceccarelli, “Performance analysis of a 3-2-1 pose estimation device,” *IEEE Trans. on Robotics*, Vol. 21, No. 3, pp. 288-297, 2005.
- [17] C. Torras, F. Thomas, M. Alberich-Carramiñana, “Stratifying the singularity loci of a class of parallel manipulators,” *IEEE Trans. on Robotics*, to appear.
- [18] P.A. Voglewede, *Measuring Closeness to Singularities of Parallel Manipulators with Application to the Design of Redundant Actuation*, PhD dissertation, Georgia Institute of Technology, 2004.